PHYSICAL REVIEW FLUIDS **7**, 103801 (2022)

Behavior of hydrodynamic and magnetohydrodynamic turbulence in a rotating sphere with precession and dynamo action

M. Etchevest, M. Fontana, and P. Dmitruk

Universidad de Buenos Aires, Facultad de Ciencias Exactas y Naturales, Departamento de Física, & IFIBA, CONICET, Ciudad Universitaria, Buenos Aires 1428, Argentina

(Received 29 April 2022; accepted 4 October 2022; published 26 October 2022)

The effect of precession in a rotating sphere filled with fluid was studied with direct numerical simulations, in both incompressible hydrodynamics (HD) and magnetohydrodynamics (MHD) scenarios. In both cases the asymptotic state and its dependence with both rotating and precession frequency was analyzed. For the MHD case no self-sustaining dynamos were found for the prograde precession case, whereas on the other hand a critical retrograde precession frequency was found above which dynamo action is self-sustained. It was also found that these correspond to small-scale dynamos with a developed turbulent regime. Furthermore, the presence of reversals of the magnetic dipole moment is observed, with greater waiting times between reversals for smaller precession frequencies.

DOI: 10.1103/PhysRevFluids.7.103801

I. INTRODUCTION

Different studies for the behavior of magnetic fields in stars and planets, and in particular the Earth, have supported the hypothesis that inside of these systems there is a flow of highly conducting materials that produces magnetic induction [1–5]. The usual framework for modeling this generation of magnetic fields from the kinetic energy of the flow is that of magnetohydrodynamic (MHD) dynamos. According to those studies, the rotatory movement of the planet can be one of the physical ingredients for these chaotic, and often turbulent, flows [6–9]. Suggested drivers for these flows, such as thermal and/or chemical effects and geometrical effects, like ellipticity, have been suggested to be relevant in the context of modeling the flows found in planet cores or stars [10]. A distinctive force that was also suggested is the precession effect in the otherwise constant rotation of the planet [6–9,11,12], a mechanism that can be responsible for the injection of kinetic energy in the system. In the dynamics of the fluid (or magnetofluid), precession can be mathematically modeled through a term in the equations of motion (Navier-Stokes or MHD) that is proportional to the time derivative of the angular velocity.

The precession effect in the full sphere was previously studied numerically, mostly in the laminar regime, as well as the transition to the turbulence regime [13]. Also, precessing spherical shells were analyzed in similar regimes [14]. Under these scenarios different types of dynamos were found, including stable dynamos, self-killing dynamos, and intermittent dynamos. It was also suggested that the turbulent regime may lead to small-scale dynamo at the surface, both in the full sphere and in the spherical shell. Another subject that deserves some consideration when studying dynamo regimes is the choice of boundary conditions [15]. In Refs. [13,14] the poloidal component of the magnetic field smoothly matches with a potential field outside, whereas the assumption of an insulating boundary leads to the vanishing of the toroidal component at the borders of the domain. Adding the no-slip boundary condition to the aforementioned choice constitutes a geodynamolike situation.

For some dynamo systems that have a preferential direction, as is the case of rotating celestial bodies, the magnetic fields arising from flow dynamics are known to undergo polarity reversals in their magnetic dipole moment [4,16–19]. We have previously studied these reversals in the context of magnetohydrodynamic equations with steady rotation [20–22]. Here we consider the influence of a nonsteady component in the angular velocity (i.e., of precession) on that phenomenon.

In this work we analyze the effect of precession on a conducting fluid inside a spherical cavity using 75 direct numerical simulations (DNS) of the MHD equations. We first consider the purely hydrodynamic equations (i.e., no magnetic field) under rotation and precession at constant frequency, and perform a parametric study to analyze the asymptotic behavior of the flow once a statistically stationary state is reached. Afterwards we proceed to analyze the magnetohydrodynamic case, starting from an initial random magnetic field and observing its evolution. We focus on the study of the turbulent regime and the presence of dynamo action, looking for self-sustaining dynamos, concentrating on the sensitivity to the rotation and precession frequency values. Furthermore, we analyze the existence of magnetic dipole reversals in the system and its behavior with the presence of precession.

The organization of the paper is as follows. Section II contains the model equations, including the initial conditions, and a description of the numerical method employed in the simulations. The results for these numerical simulations are found in Sec. III, distinguishing between the hydrodynamics (HD) and MHD cases. Finally, in Sec. IV we summarize the main results of this study.

II. SIMULATION SETUP

A. Model equations and numerical scheme

In this work we study a rotating spherical domain V filled with an incompressible conducting fluid. The boundary is considered to be rotating in a nonsteady way (i.e., precessing), with an angular velocity $\boldsymbol{\Omega} = \Omega_0[\cos(\gamma t)\sin(\alpha)\hat{\boldsymbol{x}} + \sin(\gamma t)\sin(\alpha)\hat{\boldsymbol{y}} + \cos(\alpha)\hat{\boldsymbol{z}}]$, where Ω_0 is the amplitude of the angular velocity, γ its precession frequency, and α its precession angle. The density of the fluid is taken to be uniform and equal to unity. In a noninertial reference frame that rotates fixed with the domain's boundary, the usual magnetohydrodynamic equations can be written as follows:

$$\frac{\partial \boldsymbol{v}}{\partial t} = \boldsymbol{v} \times \boldsymbol{\omega} - \nabla \mathcal{P} + \boldsymbol{J} \times \boldsymbol{B} + \nu \nabla^2 \boldsymbol{v} - 2\boldsymbol{\Omega} \times \boldsymbol{v} + \boldsymbol{r} \times \dot{\boldsymbol{\Omega}}, \tag{1}$$

$$\frac{\partial \boldsymbol{B}}{\partial t} = \nabla \times (\boldsymbol{v} \times \boldsymbol{B}) + \eta \nabla^2 \boldsymbol{B}, \tag{2}$$

$$\nabla \cdot \boldsymbol{v} = 0, \tag{3}$$

$$\nabla \cdot \boldsymbol{B} = 0, \tag{4}$$

where $\boldsymbol{v}$, $\boldsymbol{\omega}$, and $\boldsymbol{B}$ are the velocity, vorticity, and magnetic fields, respectively. $\boldsymbol{J} = \nabla \times \boldsymbol{B}$ is the current density, the total pressure is $\mathcal{P}$, and ν and η are the kinematic viscosity and the magnetic diffusivity. $\boldsymbol{r}$ is the position vector, whereas $\dot{\boldsymbol{\Omega}}$ is the time derivative of the angular velocity. Note that the last term on the right-hand side of Eq. (1) corresponds to the precession term. All quantities are expressed in dimensionless Alfvénic units.

The boundary conditions that we consider are that the normal components of $\boldsymbol{v}$, $\boldsymbol{B}$, $\boldsymbol{\omega}$, and $\boldsymbol{J}$ must all vanish in the surface of the spherical domain, $r = R = 1$ (using the ratio of the sphere R to normalize lengths). The vanishing normal component of $\boldsymbol{v}$ represents the fact that there is no mass flux across the surface. Regarding electromagnetic boundary conditions, the vanishing normal components of $\boldsymbol{B}$ and $\boldsymbol{J}$ can be considered as modeling the situation where a thin layer of dielectric material ($\boldsymbol{J} \cdot \hat{\boldsymbol{r}} = 0$) is coated on the outside by a perfect conductor ($\boldsymbol{B} \cdot \hat{\boldsymbol{r}} = 0$). The condition that results in a vorticity field tangential to the surface is implied by, but does not imply, no-slip boundary conditions. A more extensive discussion on the choice of boundary conditions can be found in Refs. [23,24]. As mentioned before, different types of boundary conditions have been previously considered in Refs. [13,14]. A related study in which we address the specific influence of the boundary conditions on the dynamo action has been considered in Ref. [15], although in a different geometry.

For the boundary conditions under consideration, the total energy balance is determined as

$$\frac{dE}{dt} = \int_V \boldsymbol{v} \cdot (\boldsymbol{r} \times \dot{\boldsymbol{\Omega}}) dV - 2\nu Z - \int_V \eta |\boldsymbol{J}|^2 dV + \int_S \nu (\boldsymbol{v} \times \boldsymbol{\omega}) \cdot \hat{\boldsymbol{n}} dS, \tag{5}$$

where $\hat{\boldsymbol{n}}$ is an outward-pointing unit vector normal to the sphere's surface. This equation can be obtained from the dynamical Eqs. (1)–(4) after multiplying by the velocity $\boldsymbol{v}$ and the magnetic field $\boldsymbol{B}$, respectively, and integrating in volume space to obtain the total energy,

$$E = \frac{1}{2} \int_V \boldsymbol{v}^2 + \boldsymbol{B}^2 dV. \tag{6}$$

The right-hand side of Eq. (5) contains the injection energy ϵ given by the precession term (first term containing the time derivative of the angular velocity), and dissipative terms like the fluid volume dissipation that involves the enstrophy $Z = 1/2 \int_V |\boldsymbol{\omega}|^2 dV$, the magnetic field dissipation involving the current density. The surface term corresponds to the injection or dissipation of energy through the boundary. This energy balance equation will be the base for the scaling models presented in the forthcoming sections.

Another important feature of magnetic fields is their topology. To study the symmetry degree of the magnetic field, the magnetic energy can be separated into each spherical harmonic contribution E_l^B,

$$E_l^B = \frac{1}{2} \sum_{q,m} |\xi_{qlm}^B|^2, \tag{7}$$

where the dipolar contribution to the magnetic energy is E_1^B, the quadrupolar one is E_2^B, and so on. The magnetic dipole moment vector $\boldsymbol{m}$ is defined as

$$\boldsymbol{m} = \int_V \boldsymbol{r} \times \boldsymbol{J} dV, \tag{8}$$

and the latitude angle of the dipole moment α is determined as

$$\alpha = \arctan\left(\frac{m_z}{\sqrt{m_x^2 + m_y^2}}\right). \tag{9}$$

We numerically integrate Eqs. (1)–(4) for the magnetohydrodynamic case and with null $\boldsymbol{B}$ for the purely hydrodynamic case using the SPHERE code [24]. In both scenarios we expand $\boldsymbol{v}$ and $\boldsymbol{B}$ in terms of Chandrasekhar-Kendall (CK) functions which constitute a spectral basis, as reported in Refs. [23,24]. These functions are the eigenfunctions of the curl with linear eigenvalue, so they obey the following expression:

$$\nabla \times \boldsymbol{K}_i = k_i \boldsymbol{K}_i. \tag{10}$$

Equation (10) can be converted into a vector Helmholtz equation, for which the three indices q, l, and m are needed to express all the solutions. The vector fields $\boldsymbol{K}_i$ can be succinctly expressed as

$$\boldsymbol{K}_{qlm} = k_{ql} (\nabla \times \psi_{qlm} \hat{\boldsymbol{r}}) + \nabla \times (\nabla \times \psi_{qlm} \hat{\boldsymbol{r}}), \tag{11}$$

with ψ_{qlm} as a solution to the scalar Helmholtz equation. Considering that our spherical domain contains the origin, the collection ψ_{qlm} is given by

$$\psi_{qlm} = C_{ql} j_l(|k_{ql}| r) \mathrm{Y}_l^m(\theta, \varphi), \tag{12}$$

where j_l is the spherical Bessel function of order l and Y_l^m is the spherical harmonic of degree l and order m. C_{ql} is a normalization constant which we adjust for the base components to be orthonormal to each other with respect to the usual inner product. The indices are limited as follows: l and m must obey usual rules for spherical harmonic indexing, that is, $l > 1$ and $-l < m < l$, whereas the index q can be any integer except for $q = 0$. Considering this, if the fields are decomposed using the CK basis, their eigenvalues are k_{ql} and satisfy $k_{-ql} = k_{ql}$, and hence CK functions with opposing values of the index q correspond to fields with opposing helicity. Making an analogy with a Fourier decomposition, the eigenvalues k_{ql} can be thought of as an analog of the wave number. The velocity and magnetic field can therefore be expressed as

$$\boldsymbol{v}(\boldsymbol{r},t) = \sum_{\substack{q=-\infty \\ q\neq 0}}^{\infty} \sum_{l=1}^{\infty} \sum_{m=-l}^{l} \xi^v_{qlm}(t)\boldsymbol{K}_{qlm}(\boldsymbol{r}), \tag{13}$$

$$\boldsymbol{B}(\boldsymbol{r},t) = \sum_{\substack{q=-\infty \\ q\neq 0}}^{\infty} \sum_{l=1}^{\infty} \sum_{m=-l}^{l} \xi^B_{qlm}(t)\boldsymbol{K}_{qlm}(\boldsymbol{r}). \tag{14}$$

The coefficients ξ_i^v and ξ_i^B only depend on time, and to obtain its evolution we use Eqs. (1) and (2) but with the fields expanded in the CK basis, obtaining the following set of ordinary differential equations:

$$\frac{d\xi_n^v}{dt} = \sum_{ij} k_j I_{ij}^n\left(\xi_i^v\xi_j^v - \xi_i^B\xi_j^B\right) + 2\sum_i \xi_i^v \boldsymbol{\Omega}\cdot\boldsymbol{\mathcal{O}}_i^n - \nu k_n^2\xi_n^v + \mathcal{B}_n\delta_{l,1}, \tag{15}$$

$$\frac{d\xi_n^B}{dt} = \sum_{ij} k_n I_{ij}^n \xi_i^v\xi_j^B - \eta k_n^2 \xi_n^B. \tag{16}$$

Here, for notation clarity, n, i, and j each represent a (q, l, m), and I_{ij}^n and $\boldsymbol{\mathcal{O}}_i^n$ are coupling arrays which obey the following expressions:

$$I_{ij}^n = \int_V \boldsymbol{K}_n^* \cdot (\boldsymbol{K}_i \times \boldsymbol{K}_j)dV, \tag{17}$$

$$\boldsymbol{\mathcal{O}}_i^n = \int_V \boldsymbol{K}_n^* \times \boldsymbol{K}_i dV. \tag{18}$$

On the other hand, the term that comes from the forcing given by the precession is defined as

$$\mathcal{B}_n = 4\sqrt{\frac{\pi}{3}}C_{q,l}\,\mathrm{sg}(k_{q,l})j_l'(|k_{q,l}|)\left(\dot{\Omega}_z\delta_{m,0} - \frac{1}{\sqrt{2}}(\dot{\Omega}_x - i\dot{\Omega}_y)\delta_{m,1}\right), \tag{19}$$

where sg is the sign function and δ the Kronecker delta.

To solve Eqs. (15) and (16) in a computer, a numerical resolution $q_{\max}$ and $l_{\max}$ has to be chosen. Given a fixed resolution, all the normalization constants C_{ql}, the eigenvalues k_i, and the coupling arrays I_{ij}^n and $\boldsymbol{\mathcal{O}}_i^n$ are computed. These tables can then be stored and used for the computation of the time-dependent coefficients. Due to the high precision used in the spatial discretization (i.e., the CK basis), Eqs. (15) and (16) are integrated in time employing a fourth-order Runge-Kutta scheme.

B. Simulations performed

We carried out 75 direct numerical simulations, varying different parameters, as explained below. All of the simulations used $q_{\max} = l_{\max} = 7$, which implies that 882 expansion coefficients are evolved in time. The temporal resolution was $\Delta t = 10^{-3}$. Half of the simulations were for the hydrodynamic case and the other half for the magnetohydrodynamic case.

TABLE I. Runs corresponding to the HD case with their respective names (ID) and relevant adimensional parameters. The difference between the two Reynolds numbers is the time in which each one was calculated, the initial Re_0 and the final Re_f. The characteristic length considered to calculate all adimensional parameters was the sphere radius, and the initial velocity is of the order of unity.

ID	Ω_0	γ	Po	Re_0	Re_f	Ek	Ro_f
HD01	1	0.1	1.0×10^{-1}	1.0×10^{2}	1.2×10^{0}	1.0×10^{-2}	1.2×10^{-2}
HD02	4	0.1	2.5×10^{-2}	1.0×10^{2}	2.0×10^{0}	2.5×10^{-3}	5.0×10^{-3}
HD03	10	0.1	1.0×10^{-2}	1.0×10^{2}	2.1×10^{0}	1.0×10^{-3}	2.1×10^{-3}
HD04	1	1	1.0×10^{0}	1.0×10^{2}	9.7×10^{0}	1.0×10^{-2}	9.7×10^{-2}
HD05	4	1	2.5×10^{-1}	1.0×10^{2}	1.7×10^{1}	2.5×10^{-3}	4.2×10^{-2}
HD06	10	1	1.0×10^{-1}	1.0×10^{2}	2.0×10^{1}	1.0×10^{-3}	2.0×10^{-2}
HD07	1	10	1.0×10^{1}	1.0×10^{2}	1.8×10^{1}	1.0×10^{-2}	1.8×10^{-1}
HD08	4	10	2.5×10^{0}	1.0×10^{2}	5.7×10^{1}	2.5×10^{-3}	1.4×10^{-1}
HD09	10	10	1.0×10^{0}	1.0×10^{2}	1.1×10^{2}	1.0×10^{-3}	1.1×10^{-1}
HD10	1	0.1	1.0×10^{-1}	3.5×10^{1}	4.1×10^{-1}	3.0×10^{-2}	1.2×10^{-2}
HD11	4	0.1	2.5×10^{-2}	3.5×10^{1}	6.2×10^{-1}	7.5×10^{-3}	4.6×10^{-3}
HD12	10	0.1	1.0×10^{-2}	3.5×10^{1}	6.7×10^{-1}	3.0×10^{-3}	2.0×10^{-3}
HD13	1	1	1.0×10^{0}	3.5×10^{1}	2.8×10^{0}	3.0×10^{-2}	8.4×10^{-2}
HD14	4	1	2.5×10^{-1}	3.5×10^{1}	5.2×10^{0}	7.5×10^{-3}	3.9×10^{-2}
HD15	10	1	1.0×10^{-1}	3.5×10^{1}	6.2×10^{0}	3.0×10^{-3}	1.9×10^{-2}
HD16	1	10	1.0×10^{1}	3.5×10^{1}	5.8×10^{0}	3.0×10^{-2}	1.7×10^{-1}
HD17	4	10	2.5×10^{0}	3.5×10^{1}	1.9×10^{1}	7.5×10^{-3}	1.4×10^{-1}
HD18	10	10	1.0×10^{0}	3.5×10^{1}	3.5×10^{1}	3.0×10^{-3}	1.0×10^{-1}

The initial conditions for the HD case consisted of exciting only the following helical modes:

$$\xi^{v}_{qlm}\Big|_{t=0} = 0.3 \quad \text{with} \begin{cases} q = \pm 1, \pm 2 \\ l = 1, 2 \\ m = 1, 2 \end{cases} \tag{20}$$

Here, the 0.3 value was chosen *ad hoc* seeking to approximately normalize the initial energy.

The angular speed Ω_0, the precession frequency γ, and the kinematic viscosity ν were varied in each simulation. Table I contains the simulations that we show in the figures in Sec. III with their corresponding names (ID) and relevant adimensional parameters. The different ν values considered were the following: $\nu = 0.01$, $\nu = 0.03$, $\nu = 0.06$, and finally $\nu = 0.1$. It should be noted that not all the simulations are contained in the table; for better understanding, only those shown in the figures are included. Other parameters that appear in the table are the initial Reynolds number (Re_0), the final Reynolds number (Re_f), the Ekman number (Ek), the final Rossby number (Ro_f) and the Poincaré number (Po). All of them were calculated considering the sphere radius as the length scale. Those characteristic numbers differ according to the moment of the run in which the typical velocity is computed. The final velocity was determined as the time average of the flow speed in the time window where the kinetic energy is steady. The parameters can be calculated as

$$\mathrm{Re}_f = \frac{v_f R}{\nu}, \quad \mathrm{Ek} = \frac{\nu}{R^2 \Omega_0}, \quad \mathrm{Ro}_f = \frac{v_f}{R \Omega_0}, \quad \mathrm{Po} = \frac{|\gamma|}{\Omega_0}. \tag{21}$$

The table also includes Re_0, which is defined similarly to Re_f but changing the final velocity v_f for the initial velocity v_0. As indicated, Po is the ratio between the precession frequency and the angular velocity.

TABLE II. Information of the MHD simulations with their name (ID) and adimensional parameters. The viscosity is the same for all runs and, in consequence, the initial Reynolds number too.

ID	Ω_0	γ	Po	Re_0	Re_f	Ek	Ro_f
MHD00	8	3	3.75×10^{-1}	1.3×10^{3}	6.6×10^{2}	1.25×10^{-4}	8.2×10^{-2}
MHD01	10	0.1	1.0×10^{-2}	1.3×10^{3}	2.9×10^{2}	1.0×10^{-4}	2.9×10^{-2}
MHD02	10	1	1.0×10^{-1}	1.3×10^{3}	3.7×10^{2}	1.0×10^{-4}	3.7×10^{-2}
MHD03	10	10	1.0×10^{0}	1.3×10^{3}	1.24×10^{3}	1.0×10^{-4}	1.24×10^{-1}
MHD04	1	-1	1.0×10^{0}	1.3×10^{3}	6.3×10^{2}	1.0×10^{-3}	6.3×10^{-1}
MHD05	1	-3	3.0×10^{0}	1.3×10^{3}	4.2×10^{2}	1.0×10^{-3}	4.2×10^{-1}
MHD06	1	-5	5.0×10^{0}	1.3×10^{3}	3.85×10^{2}	1.0×10^{-3}	3.85×10^{-1}
MHD07	8	-1	1.25×10^{-1}	1.3×10^{3}	4.1×10^{2}	1.25×10^{-4}	5.1×10^{-2}
MHD08	8	-3	3.75×10^{-1}	1.3×10^{3}	1.3×10^{3}	1.25×10^{-4}	1.6×10^{-1}
MHD09	8	-3.5	4.4×10^{-1}	1.3×10^{3}	1.6×10^{3}	1.25×10^{-4}	2.0×10^{-1}
MHD10	8	-4	5.0×10^{-1}	1.3×10^{3}	1.9×10^{3}	1.25×10^{-4}	2.4×10^{-1}
MHD11	8	-4.5	5.6×10^{-1}	1.3×10^{3}	2.3×10^{3}	1.25×10^{-4}	2.9×10^{-1}
MHD12	8	-5	6.25×10^{-1}	1.3×10^{3}	2.8×10^{3}	1.25×10^{-4}	3.5×10^{-1}
MHD13	16	-1	6.2×10^{-2}	1.3×10^{3}	4.2×10^{2}	6.25×10^{-5}	2.6×10^{-2}
MHD14	16	-3	1.9×10^{-1}	1.3×10^{3}	1.1×10^{3}	6.25×10^{-5}	6.85×10^{-2}
MHD15	16	-3.5	2.2×10^{-1}	1.3×10^{3}	1.3×10^{3}	6.25×10^{-5}	8.35×10^{-2}
MHD16	16	-4	2.5×10^{-1}	1.3×10^{3}	1.6×10^{3}	6.25×10^{-5}	1.0×10^{-1}
MHD17	16	-4.5	2.8×10^{-1}	1.3×10^{3}	1.9×10^{3}	6.25×10^{-5}	1.2×10^{-1}
MHD18	16	-5	3.1×10^{-1}	$1..3 \times 10^{3}$	2.2×10^{3}	6.25×10^{-5}	1.4×10^{-1}

On the other hand, the MHD simulations were initially excited in the following modes for the velocity field:

$$\xi^{v}_{qlm}\Big|_{t=0} = 0.5 \quad \text{with } q = 3 \begin{cases} \text{if } l = 1, 2 \Rightarrow m = 0, 1 \\ \text{if } l = 3 \Rightarrow m \in [0, 3] \end{cases} \tag{22}$$

and for the magnetic field:

$$\xi^{B}_{110}\Big|_{t=0} = 0.5, \quad \xi^{B}_{111}\Big|_{t=0} = 0.5(1 - i), \tag{23}$$

in order to have fields with net initial helicity, a feature known to favor dynamo action. The corresponding Table II shows the different runs for the MHD case. A unit magnetic Prandtl number P_m is prescribed, that is, the magnetic diffusivity η is equal to the kinematic viscosity ν in all the simulations. This differs from the typical values found in astrophysical scenarios, which are usually considered to be in the range $10^{-6} - 10^{-3}$. However, based on recent studies [15], we expect that similar regimes to the ones we report here might be attainable provided the magnetic Reynolds number Re_m is high enough. In contrast to the HD case, only the values of Ω_0 and γ were varied. In this case we also considered negative values of the precession frequency, an important fact that we discuss in Sec. III.

III. RESULTS

A. HD Results

We first report the results for the purely hydrodynamic case (i.e., no magnetic field). We performed a parametric study changing three of the parameters of the system: the rotation rate Ω_0, the precession frequency γ, and the kinematic viscous coefficient ν.

Since the torque given by the precession is forcing the system, whereas viscosity is acting as a dissipation force, it is natural to expect that at certain times the energy and enstrophy have a statistically stabile value. This is evidenced in Fig. 1, where for the two quantities a transitory

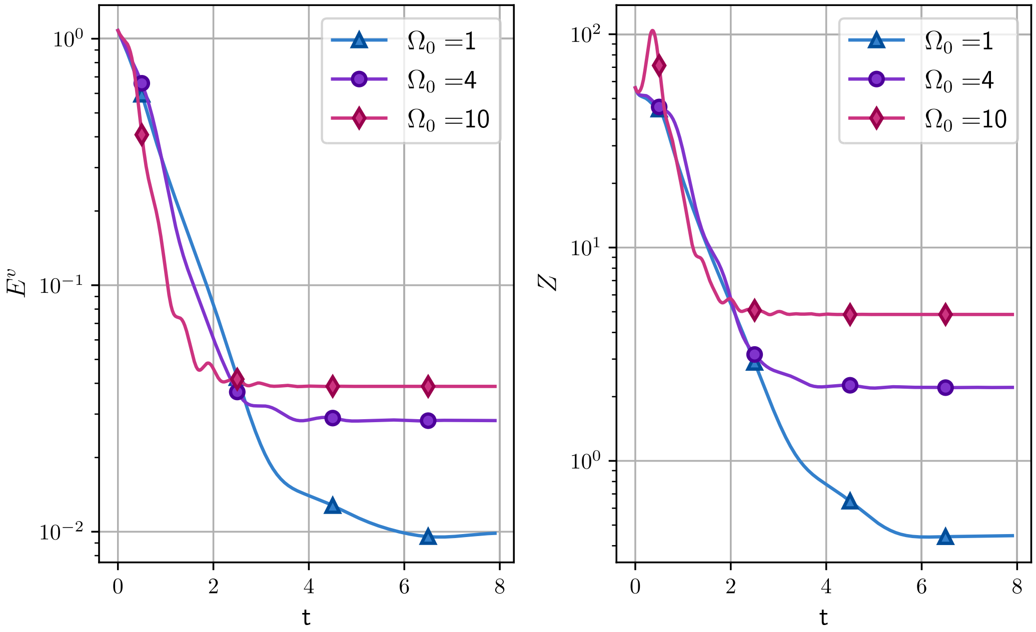

FIG. 1. Energy E_k (left) and averaged enstrophy $\langle \omega^2 \rangle$ (right) as a function of time for the runs HD04, HD05, and HD06.

regime followed by a stabilization is observed for our simulations. The transient initial decaying regime observed here is similar to previous results for the case without precession [24]. On the other hand, the presence of precession gives an asymptotic value for both the energy $\int_V \boldsymbol{u}^2 dV$ and enstrophy $\int_V \boldsymbol{\omega}^2 dV$. This asymptotic value is different for each simulation, increasing when either Ω_0 or γ are increased (i.e., more energy injected) and decreasing for larger values of ν (i.e., more energy dissipated).

In an attempt to model this asymptotic scaling we argue the following: Looking at the energy Eq. (5) without the current density that appears in the MHD case, we consider a scaling for the dissipation rate $D \approx \nu U^2/l^2$ where we chose $U = \langle v \rangle$ as a characteristic velocity of the system, and with the Taylor scale as the characteristic length $l \approx \sqrt{\nu R/U}$. This last expression is the result of considering the sphere radius ($R = 1$) as the injection length scale in the expression $l \approx \mathrm{Re}^{-1/2} R$. In the scaling for the dissipation rate we neglect any effect of the boundary term. On the other hand, we take a scaling for the energy injection rate as coming uniquely from the precession term, $\epsilon \approx R U \gamma \Omega_0$. Assuming a balance between the dissipation and the injection rate in the statistically stationary state $D \approx \epsilon$, it follows then that the energy scales as $U^2 \approx \gamma \Omega_0$.

The proposed scaling is evaluated in Fig. 2, where we show the mean kinetic energy versus the corresponding $\gamma \Omega_0$ value for that run and compare with the model (represented by a linear behavior in this plot). It can be seen that the results obtained in most of the simulations (displayed in the figure with filled symbols) are consistent with the scaling proposed. Furthermore, it can be noticed that the scaling does not match the results for the runs with $\gamma = 0.1$, represented in the figure with open symbols. This is expected, because the precession frequency is relatively small in comparison with the rotation rate Ω_0. In this case the hypothesis that the energy injection occurs solely due to the precession term may not be correct in this region of the parameter space.

As a final diagnosis for the pure hydrodynamic case in Fig. 3, we show the kinetic energy spectra for different runs varying Ω_0. It can be seen that the spectra follow a Kolmogorov-like behavior ($\sim k^{-5/3}$) at the large scales, which is consistent with the development of stationary turbulence, although the range of scales is very limited.

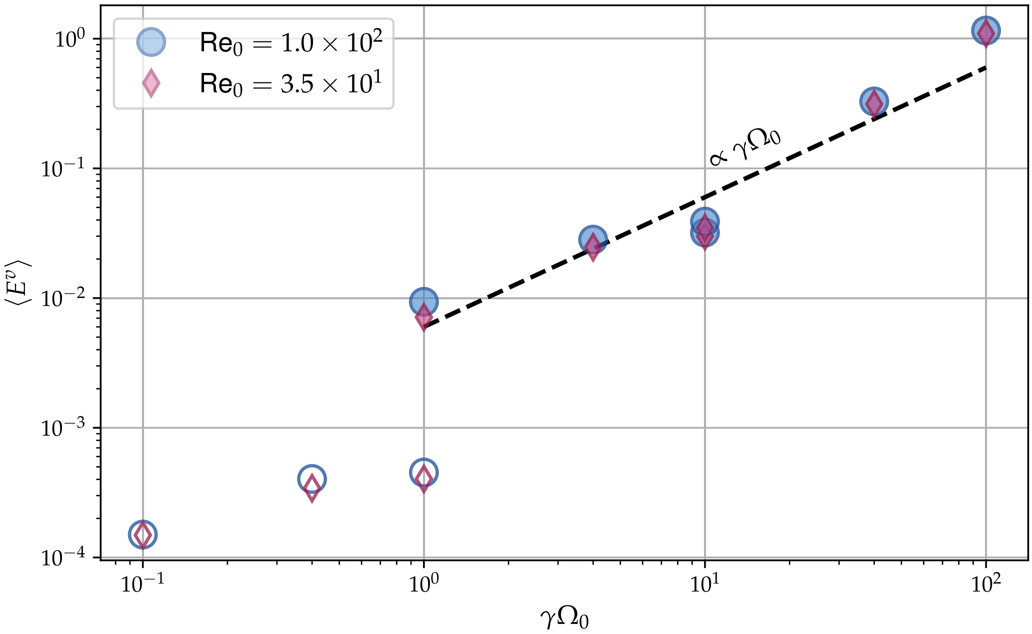

FIG. 2. Mean kinetic energy $\langle E^v \rangle$ of all the runs in Table I as a function of $\gamma\Omega_0$. The dashed line corresponds to the scaling of the proposed model, and filed and open symbols represent the runs with $\gamma \geqslant 1$ and $\gamma = 0.1$, respectively.

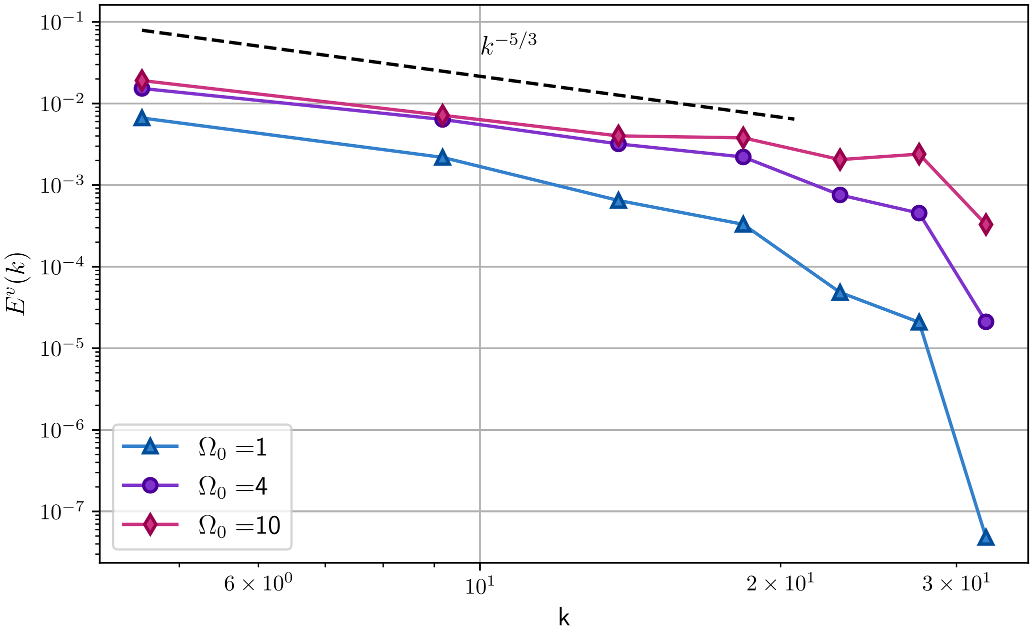

FIG. 3. Kinetic power spectra E as a function of the CK wave number k for different runs with varying Ω_0. The reference line corresponds to the Kolmogorov spectrum $k^{-5/3}$.

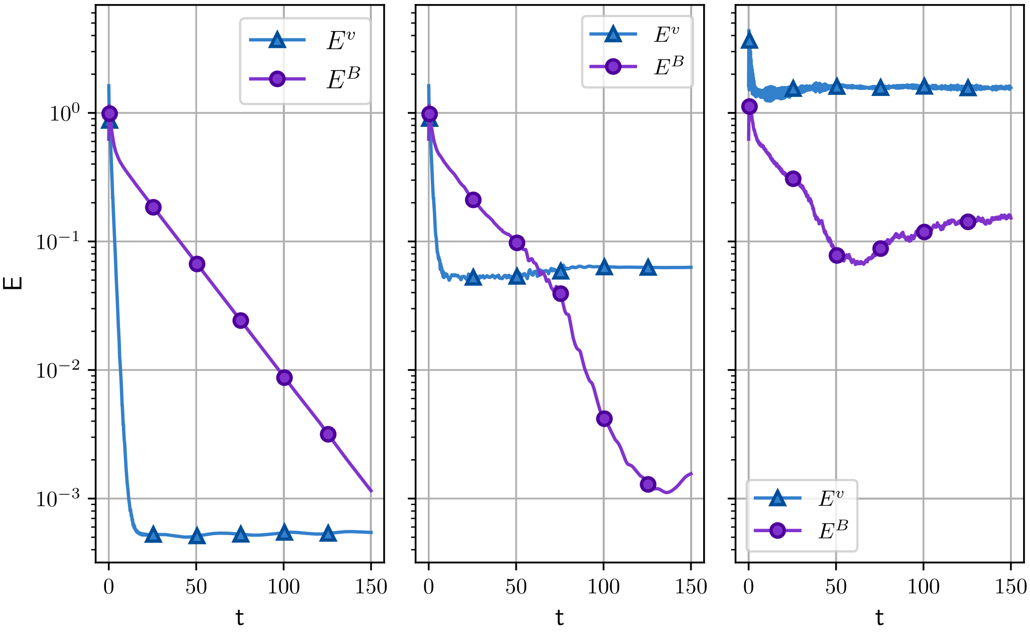

FIG. 4. Magnetic and kinetic energy as a function of time for MHD01 (left), MHD02 (middle), and MHD03 (right), which differ in the precession frequency, $\gamma = 0.1$, 1, 10, respectively, and have the same value of $\Omega_0 = 10$. It can be observed that these runs do not generate dynamos, except for very high values of Ω_0 and γ, as is the case for the MHD03 run (rightmost panel).

A related subject is the development of (inverse or direct) energy and/or enstrophy cascades. Previous studies have addressed this issue in the presence of rotation. In two-dimensional turbulence both an inverse cascade for the energy and a direct cascade for the enstrophy were observed [25,26]. For the three-dimensional case a split cascade in the energy appears, whereas the helicity (integral of velocity dot vorticity $\int_V \boldsymbol{u} \cdot \boldsymbol{\omega}\, dV$) presents a direct cascade [27]. The existence of a cascade in the angular momentum when the boundary is closed is also possible [28]. As far as we are aware, there is no study of the cascades in the presence of precession. This would be an interesting subject to address in future works.

B. MHD Results

We now consider adding a initial magnetic field to act as a seed, in order to study the feasibility of dynamo action, as well as the existence of magnetic dipole reversals. The forcing is again given by the precession term, and we vary the parameters, in this case Ω_0 and the precession frequency γ, in order to study the different behavior of the system for each case.

In Fig. 4 we show the results for the kinetic and magnetic energy as a function of time for three different runs, labeled MHD01, MHD02, and MHD03, which differ in the value of the precession frequency $\gamma = 0.1$, 1, 10, respectively, and with the same value for the rotating frequency $\Omega_0 = 10$. As it can be observed, the magnetic energy is not sustained, decaying to very low values, except for the high γ case, where nevertheless a final stationary value lower than the initial value is reached.

We then considered negative values of γ, that is, retrograde precession. A comparison of the magnetic energy versus time for both cases (prograde and retrograde precession) is shown in the left panel of Fig. 5. It can be seen that in the retrograde case the magnetic energy reaches a higher statistically stationary value than in the prograde case and it also attains it faster. The right panel of Fig. 5 shows the normalized kinetic energy spectra for both cases. The temporal average of

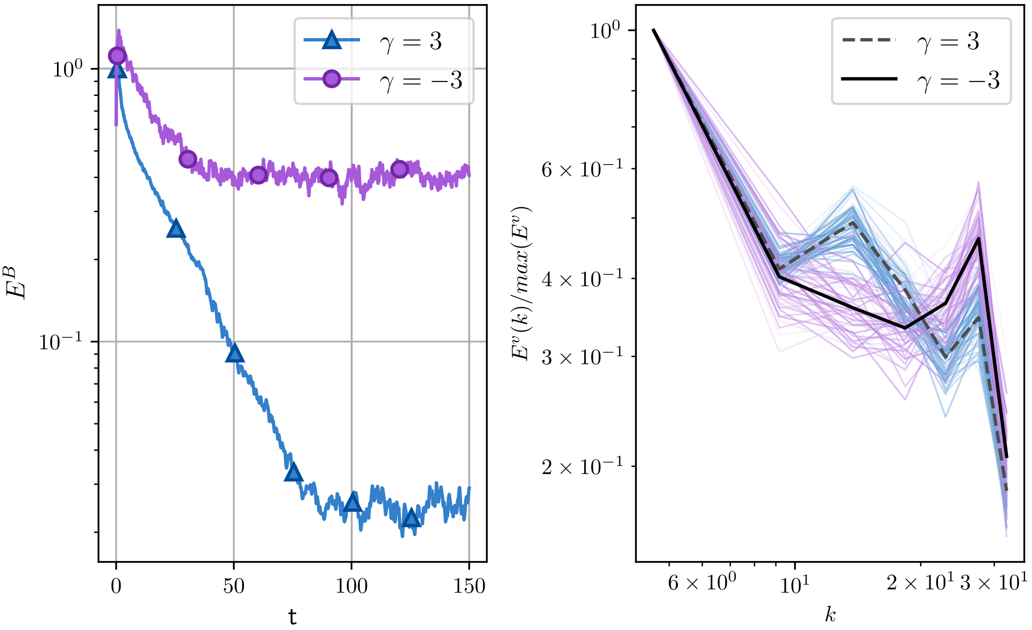

FIG. 5. Magnetic energy vs time for the prograde and retrograde cases (left); normalized kinetic energy spectra for both cases (right). The spectrum at different times is shown in colors, and the time average is shown as a dashed line for the prograde case and a solid line for the retrograde case.

the prograde case is the dashed line and the retrograde one is the solid line. A dominance of the smaller scales is noted in the retrograde case as compared with the prograde case. This indicates that a stronger turbulent regime is reached in the retrograde case and this favors the development of small-scale dynamos, as it will be more clearly shown later.

From now on the work will be focused on the retrograde precession. This case is particularly interesting, as it has been experimentally studied in several works related to the Earth's liquid core [6,8,29,30]. The results for different runs with retrograde precession are shown in Fig. 6. The leftmost panel, where the magnetic energy is not sustained, corresponds to the case with $\Omega_0 = 1$. On the other hand, in the middle panel with $\Omega_0 = 8$ dynamo action is observed for the larger values (in absolute value) of $\gamma = -3, -5$. A similar result is obtained for the case with $\Omega_0 = 16$ in the rightmost panel. A case of clear magnetic field generation (i.e., dynamo action) is observed for the $\Omega_0 > 1$ cases and for the largest values of (negative) γ. A critical precession frequency γ_c can also be appreciated which separates the self-sustaining from extinguishing dynamo regimes. This sharp transition can be found in the range $-3 < \gamma_c < -1$. Only for $|\gamma| > |\gamma_c|$ is the magnetic energy maintained at a stable level, i.e., a self-sustaining dynamo is attained.

In order to obtain a scaling for the total energy (kinetic plus magnetic) we proceed in a similar way as was presented in the HD Results subsection. We assume in this case that the injection rate is the same as the energy transfer rate (in a statistically stationary state), so $\epsilon \approx (U^3 + B^2 U)/l \approx U^3/l$, taking $U \approx B$ as the results of the runs seems to indicate. Here l is a characteristic length which can be linked with the injection rate and the rotation parameters from the scaling $\epsilon \approx l\Omega_0\gamma$ so we obtain $l \approx \epsilon/(\Omega_0\gamma)$. Replacing this scaling for l in the expression $\epsilon \approx U^3/l$, it follows then that the total energy scales as $E = U^2 + B^2 \approx 2U^2 \approx \epsilon/\sqrt{\gamma\Omega_0}$. This scaling is analyzed in Fig. 7, where the final average energy E is plotted against $\epsilon/\sqrt{\gamma\Omega_0}$ for several runs. The straight line corresponding to the perfect scaling is shown as a reference and it is notable that for this case a turbulent scaling reproduces satisfactory behavior.

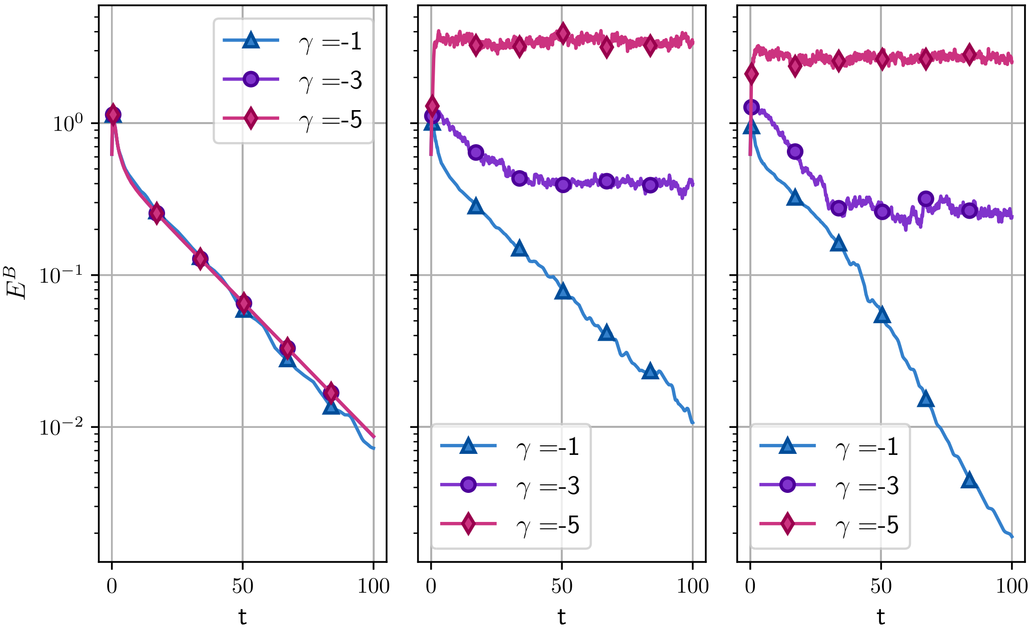

FIG. 6. Comparison of the time evolution of the magnetic energy for different γ values. Each panel is distinguished by the corresponding value of Ω_0. On the left with $\Omega_0 = 1$ are the simulations MHD04, MHD05, and MHD06; in the middle with $\Omega_0 = 8$ are MHD07, MHD08, and MHD12; and finally on the right with $\Omega_0 = 16$ are the runs MHD13, MHD14, and MHD18.

Another type of diagnosis to characterize the topology of the magnetic field is presented in Fig. 8, which shows the magnetic energy spectra for different runs, all with statistically stationary magnetic energy (i.e., self-sustaining dynamos). As can be seen, the magnetic energy seems to be dominated by the larger values of k, meaning the dynamos are in a small-scale regime.

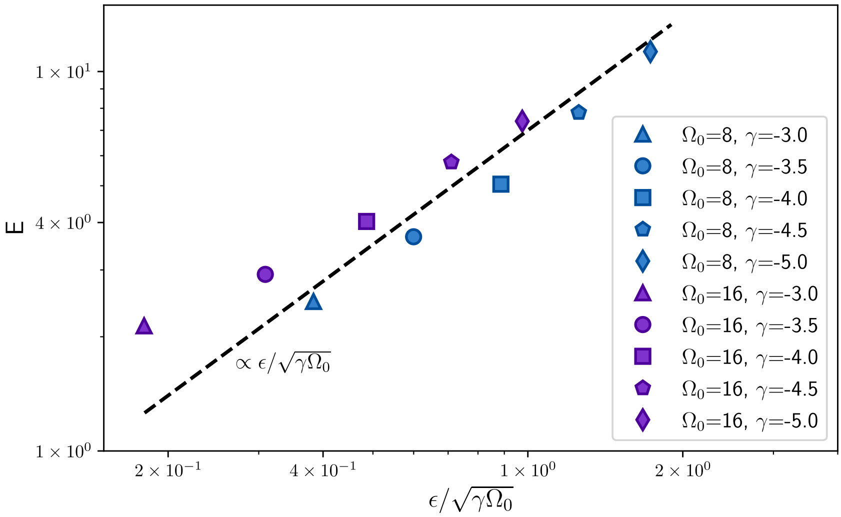

FIG. 7. Total energy as a function of the quantity $\epsilon/\sqrt{\gamma\Omega_0}$ for different runs (MHD08–MHD12 and MHD14–MHD18). The proposed scaling is indicated with a dashed line.

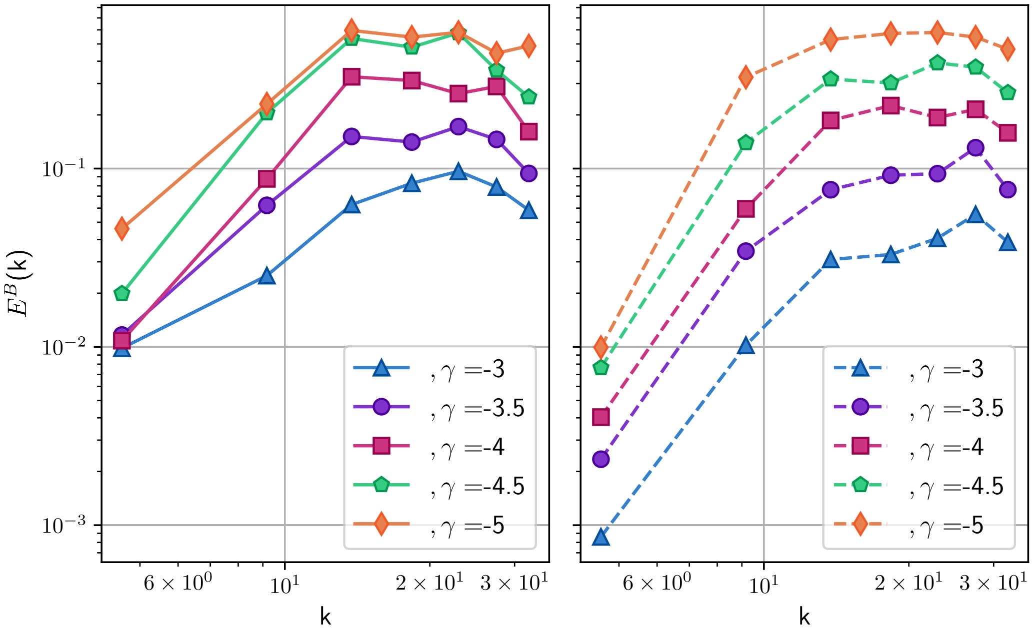

FIG. 8. Magnetic energy spatial spectra for runs with $\Omega_0 = 8$ (MHD08–MHD12) on the left and with $\Omega_0 = 16$ (MHD14–MHD18) on the right; all of them are for the time $t = 150$. A predominance in the high values of k can be observed for all of the runs. This suggests that these are small-scale dynamos.

An interesting phenomenon is the reversal of the magnetic dipole moment component parallel to the mean rotation axis m_z. We show the behavior of the normalized value $m_z/|m|$ versus time in Fig. 9 for a short time window (to better appreciate the dynamics) for a set of runs with $\Omega_0 = 8$ and different values of $\gamma = -3, -3.5, -4, -4.5, -5$, from top to bottom. The plots reveal the existence of reversals in all these dynamo runs, and it can also be seen that the dynamics seems to be faster for the larger values of $|\gamma|$. The right panel of Fig. 9 shows the normalized histograms corresponding to the distribution of times between reversals (*waiting times*). The histograms are consistent with the fact that the reversal occurs faster when the value of the precession frequency $|\gamma|$ is greater, because there is a greater domain of long waiting times for cases with smaller values of $|\gamma|$.

We analyzed the dynamics of the magnetic field during a reversal. For this purpose we estimated the amount of magnetic energy for each spherical harmonic degree E_l^B as a function of time. The result for a reversal during run MHD08 is shown in the top panel of Fig. 10 together with the magnetic dipole latitude α. It can be readily observed that the magnetic energy in the higher harmonics is greater than in the lower orders, a feature which is consistent with a small-scale dynamo scenario discussed regarding Fig. 8. Furthermore, this organization of the magnetic energy seems to remain even when a reversal occurs. This behavior was consistently found in other reversals for this run as well as other operation parameters within the self-sustaining dynamo regime. In the bottom panel of Fig. 10, the total magnetic energy E^B during the reversal is shown. It can be observed that E^B maintains an approximately steady value during the whole interval, a finding which is consistent with previous studies in other dynamos regimes (see, e.g., Ref. [22] for the case of large-scale dynamos). It can therefore be concluded that the dynamo structure does not seem to be sensitive to the reversal of the dipolar moment.

IV. DISCUSSION

In the scenario of a rotating and precessive sphere filled with fluid, the incompressible HD and MHD equations were studied by direct numerical simulations. For both cases, a Galerkin

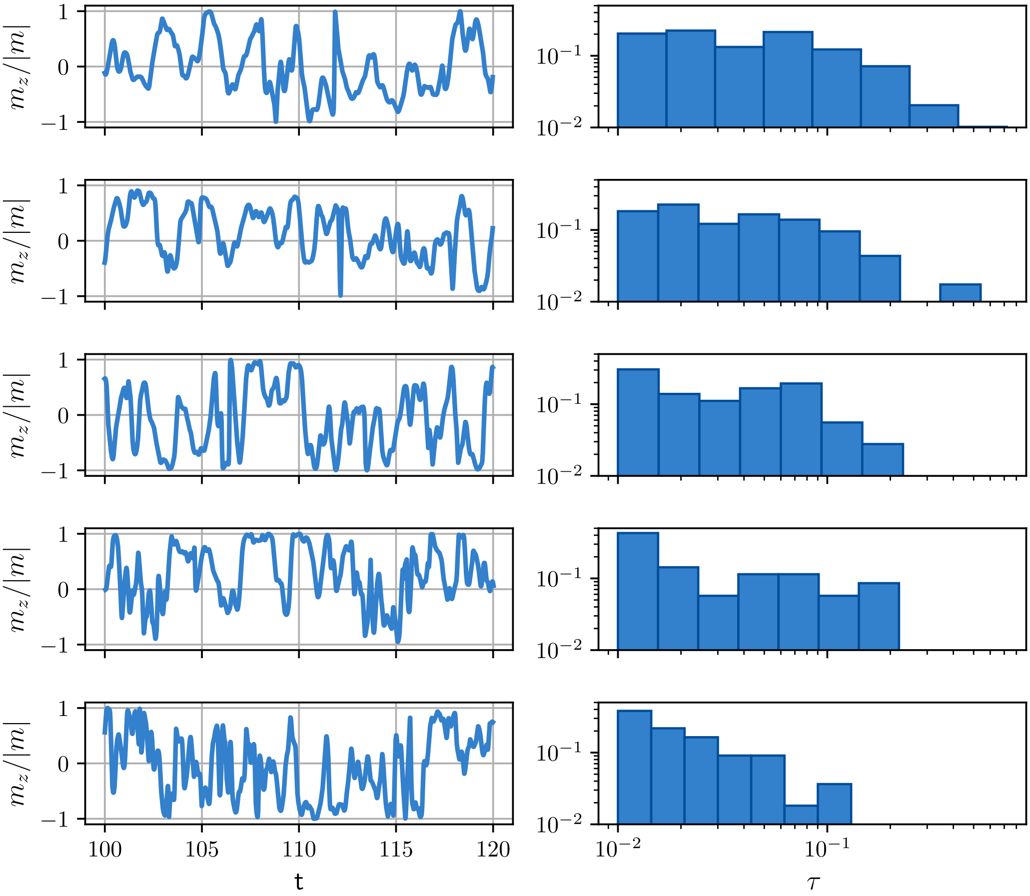

FIG. 9. Time evolution of the normalized z component of the magnetic dipole moment $m_z/|m|$ for a time window between t=100 and t=120, for all the dynamo runs with $\Omega_0 = 8$ (left) and values of $\gamma = -3, -3.5, -4, -4.5, -5$, from top to bottom. Normalized histograms of the time τ between reversals (waiting times) are shown on the right. The simulations that are shown in this figure are MHD08–MHD12.

spectral code was used. This method decomposes the fields in orthogonal Chandrasekhar-Kendall eigenfunctions. Being purely spectral, this numerical technique allowed us to integrate the system with high accuracy.

In a purely hydrodynamic setting, we found that the kinetic energy and enstrophy present a transitory regime that behaves like the nonprecessional case, after which a steady state is reached. This regime was dominated by dissipation even though the spectrum presents a power law of $k^{-5/3}$ which corresponds to the development of turbulence. We presented a model for the scaling of the kinetic energy with the parameters of the system which showed very good agreement with the results from the simulations.

For the MHD case, we separated the study into two scenarios, by taking into account the direction of precession rotation. For the case of prograde precession we could generate dynamos for high values of Ω_0 and γ. On the other hand, using retrograde precession (negative sign of the precession frequency) generates a solution with more intense turbulence in the smallest scales, and this favors the self-sustaining dynamos. For this case of retrograde precession, if the Ω_0 value is large ($\Omega_0 = 8$ or $\Omega_0 = 16$), we showed that there is a critical value of the precession frequency in order to obtain a stabilization in the magnetic energy. This critical frequency is $-3 < \gamma_c < -1$ for either of the two

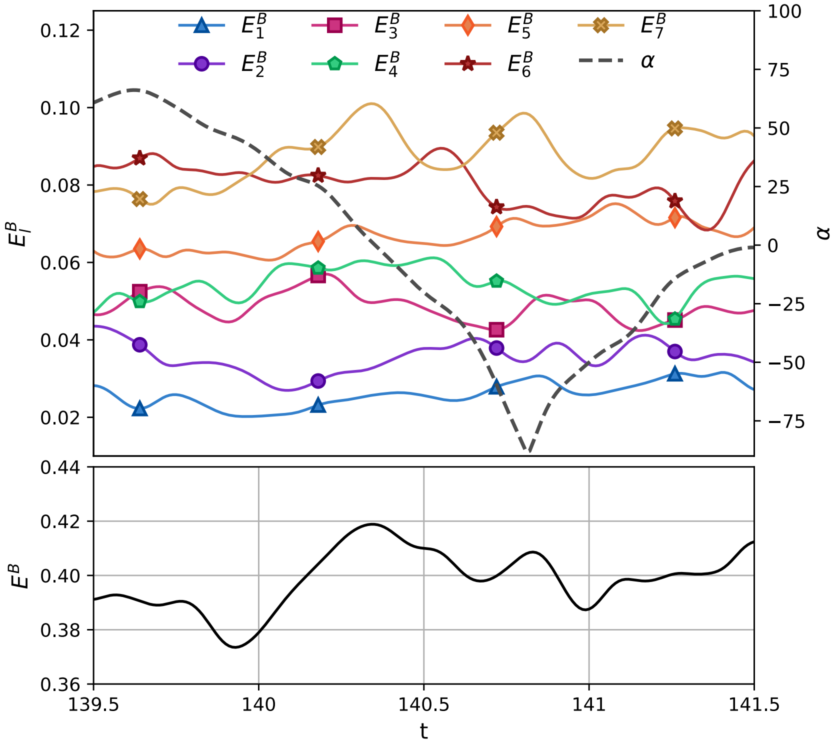

FIG. 10. (Top panel) Magnetic energy evolution during a reversal, at time $t \approx 140.4$, of the different orders of the magnetic multipole expansion (E_l^B) labeled with the subscript l, in different symbols/colors. The dashed line indicates the evolution of the magnetic dipole latitude (α). (Bottom panel) Total magnetic energy (E^B) as a function of time during the same interval. This plot corresponds to the run MHD08.

values considered for the angular velocity. Flows operating at $\gamma < \gamma_c$ showcased self-sustaining dynamos in both cases. For low rotation amplitude ($\Omega_0 = 1$) a monotonic decay of the magnetic energy was observed in the region of parameter space explored. For the MHD cases which presented sustained dynamo action, a scaling relation for the total energy in the steady state was proposed using the parameters of the problem. The proposed scaling showed a very good agreement with the results as well.

Finally, we studied the behavior of the generated magnetic field. We found that all dynamos present dominance of the small scales in the spectra of the magnetic energy, suggesting that the simulations operate in the regime of small-scale dynamos. Another interesting feature of all dynamos with a preferential direction is the presence of magnetic dipole moment reversals. Moreover, doing a statistical analysis, we observed slower dynamics in the dipole moment when the precession is also slower, i.e., when the absolute value of the frequency precession ($|\gamma|$) is smaller. Furthermore, we showed that the contribution of each spherical harmonic degree l to the magnetic energy remains equally structured over time, in a statistical sense, as previously found for small-scale dynamos [22].

The presented results constitute a contribution to the study of the influence of the precession in the turbulent dynamics of HD and MHD in a rotating sphere filled with a fluid or magnetofluid. We believe that these results show interesting features of rotating fluids with precession, including the ability to generate self-sustaining MHD dynamos with magnetic dipole reversals.

ACKNOWLEDGMENTS

The authors acknowledge support from Concejo Nacional de Investigaciones Cientificas y Tecnologicas through Grant No. 11220150100324CO and from Agencia Nacional de Promocion Cientifica y Tecnologica through Grant No. 2018-4298.

[1] G. A. Glatzmaiers and P. H. Roberts, A three-dimensional self-consistent computer simulation of a geomagnetic field reversal, Nature (London) **377**, 203 (1995).

[2] S. I. Braginsky and P. H. Roberts, Equations governing convection in Earth's core and the geodynamo, Geophys. Astrophys. Fluid Dyn. **79**, 1 (1995).

[3] P. H. Roberts and G. A. Glatzmaier, Geodynamo theory and simulations, Rev. Mod. Phys. **72**, 1081 (2000).

[4] R. Monchaux, M. Berhanu, S. Aumaître, A. Chiffaudel, F. Daviaud, B. Dubrulle, F. Ravelet, S. Fauve, N. Mordant, F. Pétrélis, M. Bourgoin, P. Odier, J.-F. Pinton, N. Plihon, and R. Volk, The von Kármán Sodium experiment: Turbulent dynamical dynamos, Phys. Fluids **21**, 035108 (2009).

[5] U. R. Christensen, J. Aubert, and G. Hulot, Conditions for Earth-like geodynamo models, Earth Planet. Sci. Lett. **296**, 487 (2010).

[6] K. Stewartson and P. H. Roberts, On the motion of liquid in a spheroidal cavity of a precessing rigid body, J. Fluid Mech. **17**, 1 (1963).

[7] F. H. Busse, Steady fluid flow in a precessing spheroidal shell, J. Fluid Mech. **33**, 739 (1968).

[8] J. Noir, P. Cardin, D. Jault, and J.-P. Masson, Experimental evidence of non-linear resonance effects between retrograde precession and the tilt-over mode within a spheroid, Geophys. J. Int. **154**, 407 (2003).

[9] A. Tilgner, Precession driven dynamos, Phys. Fluids **17**, 034104 (2005).

[10] J. Vidal and D. Cébron, Kinematic dynamos in triaxial ellipsoids, Proc. Math. Phys. Eng. Sci. **477**, 20210252 (2021).

[11] W. V. R. Malkus, Precession of the Earth as the cause of geomagnetism, Science **160**, 259 (1968).

[12] X. L. Keke Zhang, *Theory and Modeling of Rotating Fluids: Convection, Inertial Waves and Precession*, 1st ed., Cambridge Monographs on Mechanics (Cambridge University Press, Cambridge, 2017).

[13] Y. Lin, P. Marti, J. Noir, and A. Jackson, Precession-driven dynamos in a full sphere and the role of large scale cyclonic vortices, Phys. Fluids (1994) **28**, 066601 (2016).

[14] D. Cébron, R. Laguerre, J. Noir, and N. Schaeffer, Precessing spherical shells: Flows, dissipation, dynamo and the lunar core, Geophys. J. Int. **219**, S34 (2019).

[15] M. Fontana, P. D. Mininni, and P. Dmitruk, Effect of electromagnetic boundary conditions on convective dynamo onset, arXiv:2207.02394 [physics.flu-dyn].

[16] H. W. Babcock, The topology of the sun's magnetic field and the 22-YEAR Cycle, Astrophys. J. **133**, 572 (1961).

[17] Y. Ponty, H. Politano, and J.-F. Pinton, Simulation of Induction at Low Magnetic Prandtl Number, Phys. Rev. Lett. **92**, 144503 (2004).

[18] P. Olson, *Core Dynamics: Treatise on Geophysics*, 1st ed. (Elsevier, New York, 2009).

[19] H. Amit, R. Leonhardt, and J. Wicht, Polarity reversals from paleomagnetic observations and numerical dynamo simulations, Space Sci. Rev. **155**, 293 (2010).

[20] P. Dmitruk, P. D. Mininni, A. Pouquet, S. Servidio, and W. H. Matthaeus, Emergence of very long time fluctuations and $1/f$ noise in ideal flows, Phys. Rev. E **83**, 066318 (2011).

[21] P. Dmitruk, P. D. Mininni, A. Pouquet, S. Servidio, and W. H. Matthaeus, Magnetic field reversals and long-time memory in conducting flows, Phys. Rev. E **90**, 043010 (2014).

[22] M. Fontana, P. D. Mininni, and P. Dmitruk, Magnetic structure, dipole reversals, and $1/f$ noise in resistive MHD spherical dynamos, Phys. Rev. Fluids **3**, 123702 (2018).

[23] P. D. Mininni and D. C. Montgomery, Magnetohydrodynamic activity inside a sphere, Phys. Fluids **18**, 116602 (2006).

[24] P. D. Mininni, D. C. Montgomery, and L. Turner, Hydrodynamic and magnetohydrodynamic computations inside a rotating sphere, New J. Phys. **9**, 303 (2007).

[25] P. D. Mininni and A. Pouquet, Inverse cascade behavior in freely decaying two-dimensional fluid turbulence, Phys. Rev. E **87**, 033002 (2013).

[26] A. Sen, P. D. Mininni, D. Rosenberg, and A. Pouquet, Anisotropy and nonuniversality in scaling laws of the large-scale energy spectrum in rotating turbulence, Phys. Rev. E **86**, 036319 (2012).

[27] T. Teitelbaum and P. D. Mininni, Effect of Helicity and Rotation on the Free Decay of Turbulent Flows, Phys. Rev. Lett. **103**, 014501 (2009).

[28] M. López-Caballero and J. Burguete, Inverse Cascades Sustained by the Transfer Rate of Angular Momentum in a 3D Turbulent Flow, Phys. Rev. Lett. **110**, 124501 (2013).

[29] J. Vanyo, P. Wilde, P. Cardin, and P. Olson, Experiments on precessing flows in the Earth's liquid core, Geophys. J. Int. **121**, 136 (1995).

[30] M. Pais and J. Le Moeuel, Precession-induced flows in liquid-filled containers and in the Earth's core, Geophys. J. Int. **144**, 539 (2001).